nature communications

Article

https://doi.org/10.1038/s41467-024-53067-x

Light-driven integration of diazotroph-derived nitrogen in euphotic nitrogen cycle

Received: 16 May 2024

Accepted: 30 September 2024

Published online: 24 October 2024

Check for updates

Hui Shen[1], Xianhui S. Wan[1,2], Wenbin Zou[1], Minhan Dai[1], Min N. Xu[3] ✉ & Shuh-Ji Kao[1,3] ✉

The bioavailable nitrogen fixed by diazotrophs is critical for sustaining productivity in the oligotrophic ocean. Despite this, understanding how diazotroph-derived nitrogen integrates into the nitrogen cycle within the euphotic zone remains unknown. Here, we investigated nitrogen fixation rates in the particulate and dissolved fractions within the euphotic zone of the North Pacific Subtropical Gyre. Our findings reveal the proportion of nitrogen fixation rates in the dissolved fraction increases with depth. Light manipulation experiments uncover that reduced light levels can stimulate the net release of diazotroph-derived nitrogen, aligning with our depth-related observations. Furthermore, we identify two distinct transfer pathways vertically associated with light-driven ecological niches. Specifically, the released diazotroph-derived nitrogen is transferred to non-diazotrophic plankton in the upper layers. Meanwhile, in the lower layers, it contributes to the nitrification process. Our results underscore the high bioavailability of diazotroph-derived nitrogen and its rapid integration into the nitrogen cycle through multiple pathways within the well-lit ocean.

Marine nitrogen fixation, performed by diazotrophs including UCYN-A symbiosis, UCYN-B, *Trichodesmium*, etc., serves as a vital exogenous nitrogen source, sustaining primary production and contributing to export production in the oligotrophic ocean[1,2]. Even though diazotrophs comprise only approximately 1% of planktonic biomass, the ecological impacts of diazotrophs on the entire oligotrophic ecosystem are profound and rely heavily on the release and transfer of diazotroph-derived nitrogen (DDN)[3,4].

Early studies have documented the release of DDN, such as the accumulation of ammonium or dissolved organic nitrogen (DON) following *Trichodesmium* blooms in the surface ocean or enriched extracellular DON in pure cultures of *Trichodesmium*[5–7]. These studies, mainly focused on *Trichodesmium*, quantified that ~50% (with a range of 10% to 80%) of the total fixed nitrogen can be released into the dissolved pool. The release process is regulated by diazotrophic programmed cell death[8], variations in ambient light intensity[9], bacterial lysis or viral invasion[10], and zooplankton's sloppy feeding[11].

The released DDN is potentially biologically available for surrounding planktonic communities in the oligotrophic ocean. Evidence of relatively low $\delta^{15}N$ in phytoplankton or zooplankton indicates significant transfer of DDN to the planktonic food web[12,13]. Yet, the pathway and transfer rates remain poorly identified in a quantitative way due to methodological limitations, particularly the overlap in size-spectrum between diazotrophs and non-diazotrophs[14].

Studies utilizing size-fractionated techniques coupled with $^{15}N_2$ labeling incubation, mainly during surface *Trichodesmium* blooms, have shown that 5–10% of nitrogen fixed by *Trichodesmium* (recovered in the size fraction >10 μm) was transferred to small-sized (recovered in the size fraction <10 μm) non-diazotrophic biota[9,15]. Recently, high-resolution nanometer-scale secondary ion mass spectrometry has been employed to identify and quantify the transfer of released DDN into specific groups of phytoplankton and bacteria in the surface ocean, demonstrating transfer ranging from 6-21% of fixed nitrogen to diatom, pico-phytoplankton, and bacteria[14,16,17].

[1]State Key Laboratory of Marine Environmental Science & College of Ocean and Earth Sciences, Xiamen University, Xiamen, China. [2]Department of Geosciences, Princeton University, Princeton, NJ 08544, USA. [3]State Key Laboratory of Marine Resource Utilization in South China Sea, School of Marine Science and Engineering, Hainan University, Haikou, China. ✉e-mail: minxu@hainanu.edu.cn; sjkao@hainanu.edu.cn

In the field, the released DDN is partially transferred into the surrounding biota with the remainder in the dissolved fraction. Yet, the nitrogen fixation rates in the dissolved fraction (NFR_D) have been underexplored in previous studies, potentially leading to an underestimation of total nitrogen fixation rates[18]. Limited observations of NFR_D have primarily focused on surface waters in the field rather than the entire euphotic zone[19].

Considering that DDN is typically in the reduced state, existing as DON or ammonium[5,14,15], and the influence of light on the flow pathways of reduced inorganic nitrogen within the vertical gradient of light intensity in the euphotic zone[20], a question arises regarding how DDN is incorporated vertically into the nitrogen cycle throughout the entire euphotic zone.

In this study, we utilize $^{15}N_2$ isotope labeling techniques with a sophisticated experimental design to accurately quantify the nitrogen fixation rates in both particulate and dissolved fractions (NFR_P & NFR_D) across a vertical scale from the ocean's surface down to a depth of 0.1% surface photosynthetically active radiation (sPAR) in the North Pacific Subtropical Gyre (NPSG) (Supplementary Fig. 1). We also conducted pilot tests to verify the methodological reliability (Supplementary Fig. 2). Moreover, we separate the total nitrogen fixation rates (TNFR; i.e., NFR_D plus NFR_P) into those mediated by large-sized (>10 μm) and small-sized (<10 μm) diazotrophs (Supplementary Fig. 3), and the NFR_D into nitrate/nitrite (NO_x^-) and DON/ammonium. With the support of light manipulation experiments, our results provide robust evidence highlighting the significance of DDN release across the entire euphotic zone and reveal how light intensity simultaneously regulates the production, release, and transfer processes. Furthermore, we propose two vertically light-driven transfer pathways for released DDN within the euphotic zone, thus elucidating how released DDN incorporates into the intricate marine nitrogen cycle within the sunlit zone.

Results and discussion

DDN is efficiently released in the entire euphotic zone

In our study, we conducted parallel measurements of the NFR_D and NFR_P across the euphotic zone in 14 stations in the NPSG, during both the summer and the winter cruises (Supplementary Fig. 1; Supplementary Table 1). Overall, the vertical profiles of NFR_P and TNFR exhibited an unimodal pattern, with peak rates typically occurring at ~50 m (Fig. 1a, b; Supplementary Fig. 4), consistent with previous findings in the oligotrophic ocean[21–23]. The ratios of NFR_D to TNFR varied widely from 3% to 97%, with an average of 31% and a median of 52% ($n = 48$). Interestingly, the NFR_D/TNFR increased with depth (Fig. 1c, d; Supplementary Fig. 4), indicating efficient release of DDN by diazotrophs into the surrounding environment, despite the lack of clear vertical variation of NFR_D across all stations.

Furthermore, depth-integrated total nitrogen fixation rates (ITNFR) exhibited spatial variability within the NPSG (Fig. 1e; Supplementary Table 2). During the summer cruise, ITNFR in central NPSG (428 ± 75 μmol N m^{-2} d^{-1}, $n = 5$) were significantly higher than those in the northern and southern regions (76 ± 18 μmol N m^{-2} d^{-1}, $n = 3$; $p < 0.001$), whereas in the winter cruise, the differences were less pronounced ($p = 0.236$; 220 ± 149 μmol N m^{-2} d^{-1} in the central NPSG ($n = 4$) and 369 ± 98 μmol N m^{-2} d^{-1} in the northern and southern NPSG ($n = 2$)). However, ITNFR did not show significant seasonal variation across the oligotrophic NPSG (296 ± 190 μmol N m^{-2} d^{-1}, $n = 8$, in the summer; 270 ± 145 μmol N m^{-2} d^{-1}, $n = 6$, in the winter; $p > 0.05$). Depth-integrated NFR_D ($INFR_D$) accounted for 3–53% (average of 26%, $n = 14$) of ITNFR (Fig. 1e; Supplementary Table 2), indicating potential underestimation of ITNFR by ~26% when not considering $INFR_D$. Stations with lower ITNFR tended to have a higher proportion of $INFR_D$ (Supplementary Fig. 5), highlighting the importance of accounting for NFR_D in the assessment of marine nitrogen fixation rates, particularly in regions with relatively lower NFR_P.

In the vertical profile, TNFR had a significantly positive correlation with total *nifH* gene abundance at corresponding depths ($p < 0.05$; Supplementary Fig. 7a). Similarly, in the horizontal distribution across the integrated water column, ITNFR exhibits a significantly positive correlation with depth-integrated total *nifH* gene abundance at corresponding stations ($p < 0.05$; Supplementary Fig. 7b). At the central and southern NPSG stations, UCYN-B dominates in the water column, with *Trichodesmium* as the second most abundant species, revealing a coherent pattern with ITNFR (Fig. 1e, f) regardless of seasonal variations. In contrast, UCYN-A symbiosis contributes most to the *nifH* gene abundance in the water column of the two northern NPSG stations, potentially contributing to the observed TNFR there (Fig. 1e, f). The spatial distribution of UCYN-A symbiosis and UCYN-B is likely highly influenced by water temperatures (Supplementary Fig. 1c, d; Supplementary Table 1) due to UCYN-A symbiosis' adaptation to low temperatures and UCYN-B's preference for warm seawater[1,22,23]. Overall, in this study area, NFR_P is determined by the *nifH* gene abundance of UCYN-B, while NFR_D shows no clear association with any diazotroph species, in both specific layers and water column integration (Supplementary Fig. 7a, b). However, we cannot rule out the potential direct contribution of unknown diazotrophic ultramicrobacteria or viruses to the NFR_D.

Considering that photoautotrophic diazotrophs (UCYN-A symbiosis, UCYN-B or *Trichodesmium*) dominated in our study region (Fig. 1f; Supplementary Fig. 6), and total *nifH* gene abundance and the TNFR were positively correlated with light intensity at corresponding depths (Supplementary Fig. 7a), we propose that light intensity likely influences both the vertical distribution and activity of diazotrophs. Interestingly, during the summer and winter cruises, maximum TNFR often occurred at 50 m (the corresponding daily mean light intensity was about 145 μmol E m^{-2} s^{-1}) (Supplementary Fig. 8a, b; Supplementary Table 2). Given that the mixed layer depths exceeded 50 m depth at most stations in this study (Supplementary Fig. 1c–f; Supplementary Table 2) and physical-chemical parameters (such as temperature, salinity, nutrients, etc.) other than light intensity were relatively homogeneous within the mixed layer, these suggest that high surface light intensity may suppress TNFR, contributing to the observed unimodal TNFR distribution on the vertical scale. While the NFR_D did not show significant correlation with environmental parameters or diazotrophic compositions (Supplementary Fig. 7a), the NFR_D/TNFR was positively correlated with depth and negatively correlated with light intensity, possibly due to light attenuation with depth (Supplementary Fig. 8c, d).

Light intensity shapes vertical nitrogen fixation rates and portion of net release

During the winter cruise, we conducted light manipulation experiments for three stations to test our hypothesis. The results unveiled an unimodal distribution of the TNFR in response to variable light intensities (Fig. 2; Supplementary Fig. 9), consistent with the observed in situ profiles of TNFR (Supplementary Fig. 8a, b). The optimum light intensities (I_k) at layers dominated by UCYNs ranged from 12 μmol E m^{-2} s^{-1} to 81 μmol E m^{-2} s^{-1} (47 ± 22 μmol E m^{-2} s^{-1}, $n = 10$), determined from data fitting (Supplementary Fig. 9; Supplementary Table 3). The I_k values were aligned closely with previous reports for UCYN-A symbiosis (44 ± 23 μmol E m^{-2} s^{-1})[24], albeit slightly lower than those for UCYN-B (88 ± 13 μmol E m^{-2} s^{-1})[25]. Importantly, I_k showed no significant vertical variation and remained consistent among the three stations with different diazotrophic compositions. Layer exhibited the highest TNFR where in situ light intensity closely matched I_k at the depth (Supplementary Table 3). Nitrogen fixation in layers above the depth with I_k experienced light inhibition, while those below were light-limited. These findings demonstrate the pivotal role of light intensity in shaping the vertically unimodal distribution of TNFR.

https://doi.org/10.1038/s41467-024-53067-x

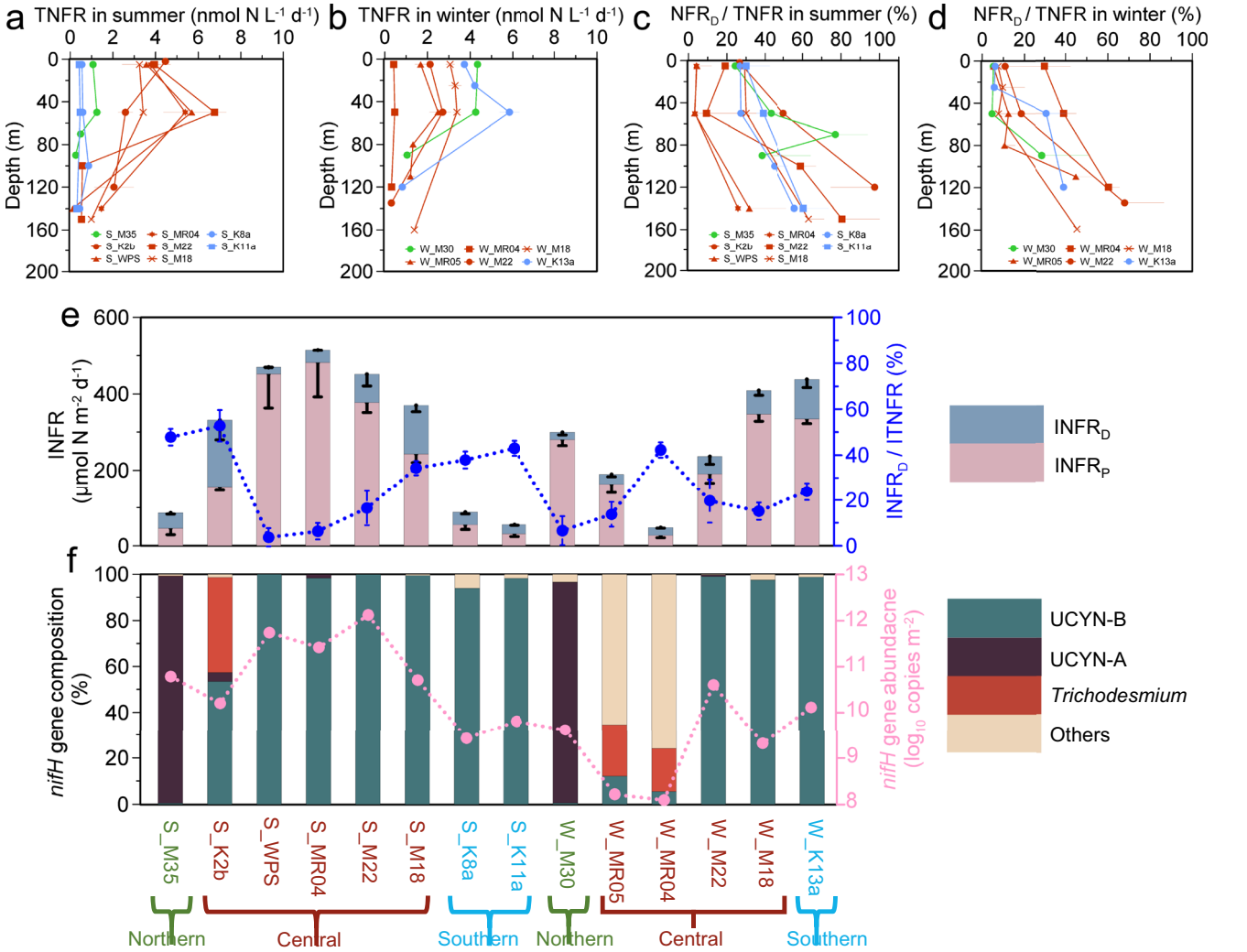

Fig. 1 | Seasonal nitrogen fixation rates and *nifH* gene abundance in all stations in the North Pacific Subtropical Gyre (NPSG). a, **b** The profiles of total nitrogen fixation rates (TNFR) during the summer and the winter cruise, respectively. Data are presented as mean values ± standard deviation. The error bars depict propagated standard deviation from triplicate rate measurements ($n = 3$ biologically independent samples). **c**, **d** the ratio of nitrogen fixation rates in dissolved fraction (NFR_D) to TNFR during the summer and the winter cruise, respectively. Data are presented as mean values +/− standard error of mean. The error bars represent the standard error of mean, with propagated standard deviation derived from triplicate rate measurements ($n = 3$ biologically independent samples). **e** The pink and blue bars represent depth-integrated nitrogen fixation rates in particulate fraction ($INFR_P$) and depth-integrated NFR_D ($INFR_D$), respectively. Data are presented as mean values − standard deviation. The error bars depict propagated standard deviation from triplicate rate measurements ($n = 3$ biologically independent samples). The deep blue dots represent the ratio of $INFR_D$ to ITNFR. Data are presented as mean values ± standard error of mean. The error bars are standard error of mean, with propagated standard deviation derived from triplicate rate measurements ($n = 3$ biologically independent samples). **f** The bars show *nifH* gene composition of targeted diazotrophs in every layer at each station. The dark green bars are UCYN-B; the dark purple bars are UCYN-A symbiosis (short for UCYN-A), including UCYN-A1 and UCYN-A2; the red bars are *Trichodesmium*; the creamy white bars are Other diazotrophs, 'Others' include UCYN-C, γ-24774A11, het1, het2, and het3. The pink dots are depth-integrated total *nifH* gene abundance (Units (copies m^{-2}) are converted to $\log_{10}$ (copies m^{-2})). **a**–**d** the prefix of the station's names: 'S' denotes stations in the summer cruise, while 'W' denotes stations in the winter cruise. The colors of the station's names and dots-lines in **a**–**d** represent the region of the stations: green, the northern NPSG; red, the central NPSG; blue, the southern NPSG. Source data are provided as a Source Data file.

In every individual layer, the NFR_D/TNFR exhibited a concave trend, contrary to the TNFR trend observed in the light manipulation experiments (Fig. 2). The NFR_D/TNFR were relatively higher under low light intensities (1 and 14 μmol E m^{-2} s^{-1}; corresponding to the in situ depths of 0.1% and 1% sPAR, lower than I_k in this study) compared to moderate light intensities (145, 290, and 745 μmol E m^{-2} s^{-1}; corresponding to the in situ depths of 10%, 20% and 50% sPAR), consistent with our in situ observations at deeper depths (Fig. 2; Supplementary Fig. 8c, d). One study has documented that under low light conditions, diazotrophs released a larger proportion of DDN into the environment[9]. It is hypothesized that surrounding organisms are unable to effectively utilize the released DDN under low light conditions, leading to the retention of released DDN in the dissolved fraction. This may result in an elevated proportion of NFR_D under low-light incubation in our light manipulation experiments. Similarly, under high-light incubations (1194 μmol E m^{-2} s^{-1}; corresponding to the in situ 2 m depth; Supplementary Table 1), the NFR_D/TNFR was higher than under moderate light intensity (Fig. 2). This excess of energy led to the increased discharge of cellular nitrogen to prevent photodestruction and light inhibition of diazotrophs and non-diazotrophic photoautotrophic phytoplankton[26], resulting in relatively low TNFR (Fig. 2) and ineffective planktonic utilization despite release, leading to the accumulation of released DDN.

Our results imply that the light intensity regulates nitrogen fixation and its net release, which may arise from the altered physiological characteristics of diazotrophs and surrounding phytoplankton. Our

https://doi.org/10.1038/s41467-024-53067-x

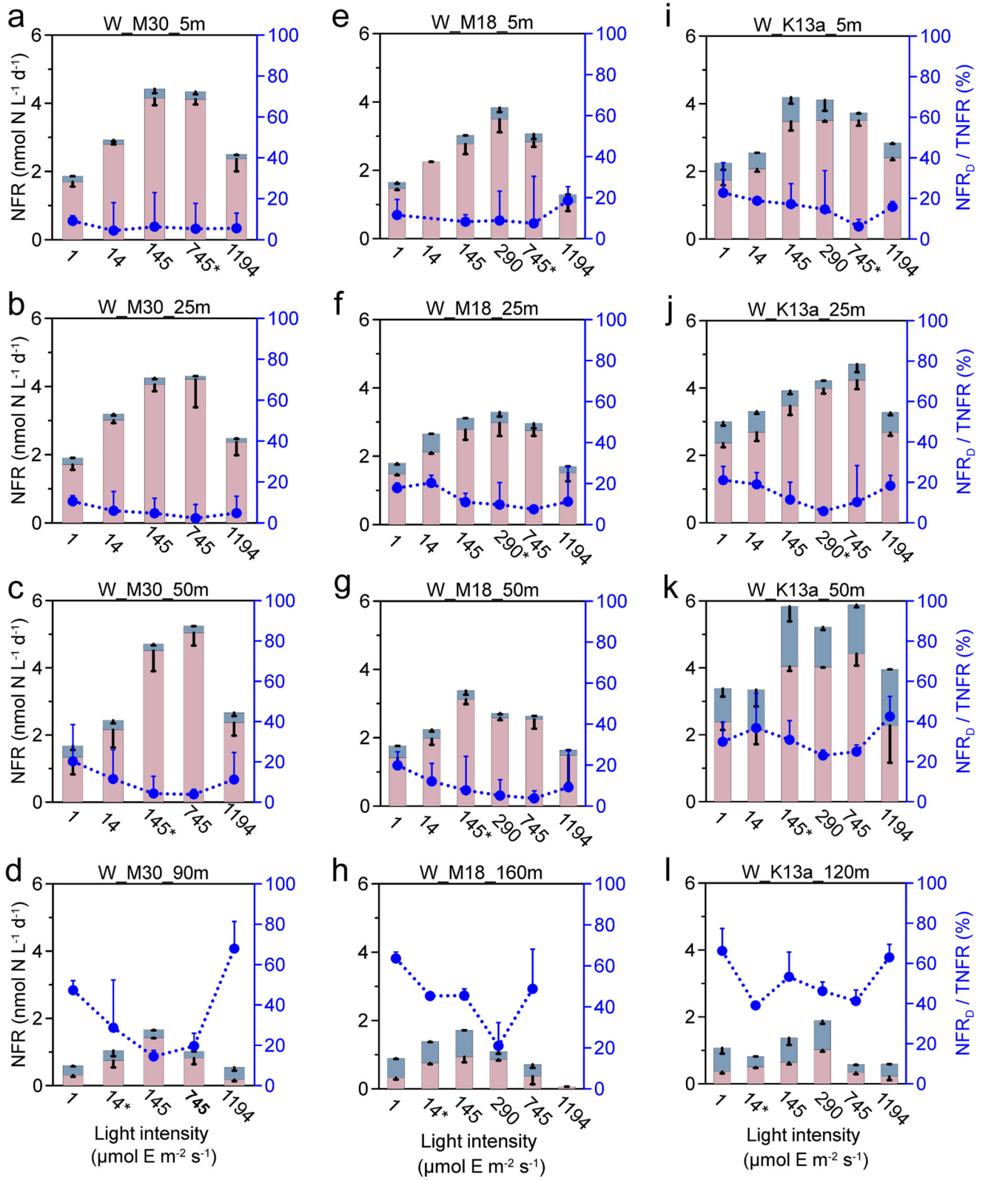

Fig. 2 | The results of light manipulation experiments in three stations during the winter cruise. Responses of nitrogen fixation rates to variable light intensities at four depths in M30 (**a**–**d**), M18 (**e**–**h**), and K13a (**i**–**l**). The pink and blue bars represent nitrogen fixation rates in particulate fraction (NFR_P) and in dissolved fraction (NFR_D). Data are presented as mean values – standard deviation. The error bars depict the standard deviation of NFR_P and NFR_D from triplicate rate measurements ($n = 3$ biologically independent samples). The deep blue dots denote the ratio of NFR_D to total nitrogen fixation rates (TNFR). Data are presented as mean values + standard error of mean. The error bars are the standard error of the mean, with propagated standard deviation derived from triplicate rate measurements ($n = 3$ biologically independent samples). The light intensity in each chart is the daily mean light intensity. The numbers with stars on the *X* axis show the in situ light intensity at the corresponding layer. Source data are provided as a Source Data file.

experiments reproduced the downward-increasing trend of in situ observation of vertical NFR_D/TNFR as light intensity attenuated (Fig. 1c, d; Fig. 2). However, the magnitude of NFR_D/TNFR in the light manipulation experiments conducted in the high light layers (≥10% sPAR) was significantly lower than that in the low light layers (<10% sPAR) regardless of the variable light intensities applied ($p \le 0.001$; Supplementary Fig. 10a–c). Similarly, in the in situ observation, the NFR_D/TNFR in the high light layers were also significantly lower than that in the low light layers ($p < 0.001$; Supplementary Fig. 10d). These distinctions suggest that while changes in light intensity contribute to the variation in NFR_D/TNFR, they alone cannot fully explain the high ratios observed under in situ low-light conditions in the low light layers.

Released DDN comprises reduced nitrogen compounds (such as DON or ammonium)[5,14,15]. Historically, labile DON uptake in marine ecosystems has been attributed to heterotrophic bacterial production[27]. Enhanced heterotrophic bacterial production was also observed during a *Trichodesmium* bloom, indicating that released DDN was transferred to bacteria[28]. In fact, the newly released DON may contribute to the labile DON pool for microbial consumption and can be transformed into ammonium by bacteria. Previous studies have shown that ammonium was preferentially utilized by phytoplankton in the high light layers, conversely, ammonium was utilized by nitrifiers and converted into NO_x^- in the dissolved pool in the low light layers[20,29]. In the euphotic zone, the vertical light gradient obviously creates niches for various microbes, including photoautotrophs and chemoautotrophs. Therefore, pathways of the released DDN could be controlled by niche differentiation.

Light-driven transfer pathways of released DDN

To test the two speculative transfer pathways of released DDN in the high light layers and low light layers, we conducted size-fractionated experiments and measured the NFR_D in the NO_x^- fraction from in situ incubations. The results from size-fractionated experiments revealed that 15–39% of fixed nitrogen from the large-sized diazotrophs (>10 μm) was transferred to small-sized biota (<10 μm) in the high light layers (Fig. 3a–c; Supplementary Fig. 11). It's worth noting that this method exclusively quantifies the transfer of released DDN from large-sized diazotrophs, implying that the mentioned transfer efficiencies present conservative estimates because we can not quantify the transfer of released fixed nitrogen derived from small-sized diazotrophs. Despite the relatively low NFR_D/TNFR (Fig. 1c, d) and the significantly lower nitrification rates in the high light layers[20,29], our results underscore that the released DDN is rapidly assimilated by surrounding ammonium-favoring phytoplankton or bacteria. The NFR_P observed encompasses both diazotrophs and non-diazotrophic plankton, indicating a direct contribution of nitrogen fixation to regenerated production within the high light layers.

In the in situ incubation, upon introducing $^{15}N_2$ into samples from the low light layers at nine stations (where the NO_x^- concentration at the remaining five stations fell below the detection limit), notable augmentations of ^{15}N in NO_x^- were observed (Supplementary Table 4). This signifies that, on average, 70% ($n = 9$) of NFR_D resided in the NO_x^- within the low light layers (Fig. 3d; Supplementary Table 5). The observation implies the released DDN entered into the nitrification process or underwent bacterial ammonification beforehand within the low light layers. Additionally, the proportion of NFR_D in the NO_x^- fraction at the low light layer (at 120 m in W_K13a) declined with increasing light intensity during our light manipulation experiments (Fig. 3e), corroborating the pathway of transferred DDN to nitrification, especially considering the light inhibition of nitrification rates[29]. Consequently, these findings validate that within the low light layers, released DDN is transferred to NO_x^- primarily through nitrifiers.

Diazotrophs demonstrate remarkable efficiency in releasing DDN, which promptly participates in the nitrogen cycling processes within the euphotic zone, as evidenced by detectable signals within 24-hour incubation. This involvement includes contributions to bacterial production, regenerated production, and nitrification. Moreover, the delineated transfer pathways within the two regimes of the euphotic zone, particularly the transfer to the nitrification process in the low light layers, play a pivotal role in the retention of released DDN in the dissolved fraction. Additionally, diazotrophs may experience greater predation pressure in low-light layers than in high-light layers[30]. Sloppy feeding by zooplankton could increase the release of DDN[11]. Consequently, this mechanism may also contribute to the observed high in situ NFR_D/TNFR in the deeper layers.

Previous studies have consistently shown that the majority of released DDN appears as DON[5,14]. Within the euphotic zone in this study, total dissolved nitrogen concentrations typically range between 3 and 5 μmol N L^{-1} (Supplementary Fig. 12). However, the nitrogen fixation rates did not surpass 10 nmol N L^{-1} d^{-1} over a 24-hour incubation period (Fig. 1a, b). The detectable transfer signal suggests that released DDN, as the majority of DON, enters into a relatively large ambient DON pool and is preferentially utilized by surrounding organisms. Additionally, the nitrogen isotopic values derived from $^{15}N_2$ labeling were also detectable in the NO_x^- within the low light layers, given that NO_x^- comprises a small proportion of total dissolved nitrogen (ranging from 0.71% to 37.71%, $n = 9$, Supplementary Table 5), which solidifies the notion of preferential utilization of released DDN. Considering the spectrum of liability within the DON pool, it ranges from truly refractory components persisting for years to millennia to highly labile forms such as urea, amino acids, and nucleic acids, which turn over in minutes to days[31–33]. The newly released DDN likely falls within the relatively more labile DON or ammonium. Thus, our results underscore the potential high bioavailability and rapid turnover of released DDN, highlighting the crucial role of diazotrophs in oligotrophic oceanic ecosystems.

Nitrogen is a crucial factor limiting marine primary production[34], and nitrogen fixation plays a pivotal role in generating bioavailable nitrogen[1]. Historically, NFR_D has been overlooked in marine nitrogen budget assessments, leading to an underestimate of the new nitrogen source in global budgets that rely solely on NFR_P[18]. Incorporating NFR_D could potentially increase the global marine nitrogen fixation budget from 223 Tg N y^{-1} (data from ref. 18) to 281 Tg N y^{-1} based on an average ratio of $INFR_D$/ITNFR of 26%. This adjustment may help reconcile debates on the imbalance of the marine nitrogen budget on a global scale and suggests a need to reassess the biogeographical distribution of marine nitrogen fixation rates[35–37].

Nitrogen fixation has long been recognized as a new nitrogen alongside atmospheric nitrogen deposition and upwelled subsurface nitrate in the euphotic zone, supporting export production in the vast oligotrophic oceans[1,2]. Our findings indicate that released DDN rapidly enters the regenerated nitrogen cycle within the euphotic zone, suggesting that nitrogen fixation's role as new nitrogen extends over longer timescales. In the short term, however, nitrogen fixation primarily acts as regenerated nitrogen. Our results demonstrate that newly fixed nitrogen is preferentially utilized by the surrounding organisms, highlighting the role of diazotrophs in sustaining primary production through the release of DDN. Our data further reveal that nitrogen fixation contributes ~1–29% of primary production (Supplementary Table 6), even though diazotrophs constitute <1% of the overall phytoplankton community[3], underscoring a considerable contribution of DDN to primary production and carbon cycle in the oligotrophic ocean.

In the low light layers, released DDN enters the nitrification pathway, contributing ~3–9% of nitrification (Supplementary Table 7). Our study provides insights into the source of nitrate in the lower euphotic zone through the shortcut of released DDN-nitrification processes, indicating that nitrogen fixation indirectly contributes new nitrogen through nitrification. This finding challenges previous studies

https://doi.org/10.1038/s41467-024-53067-x

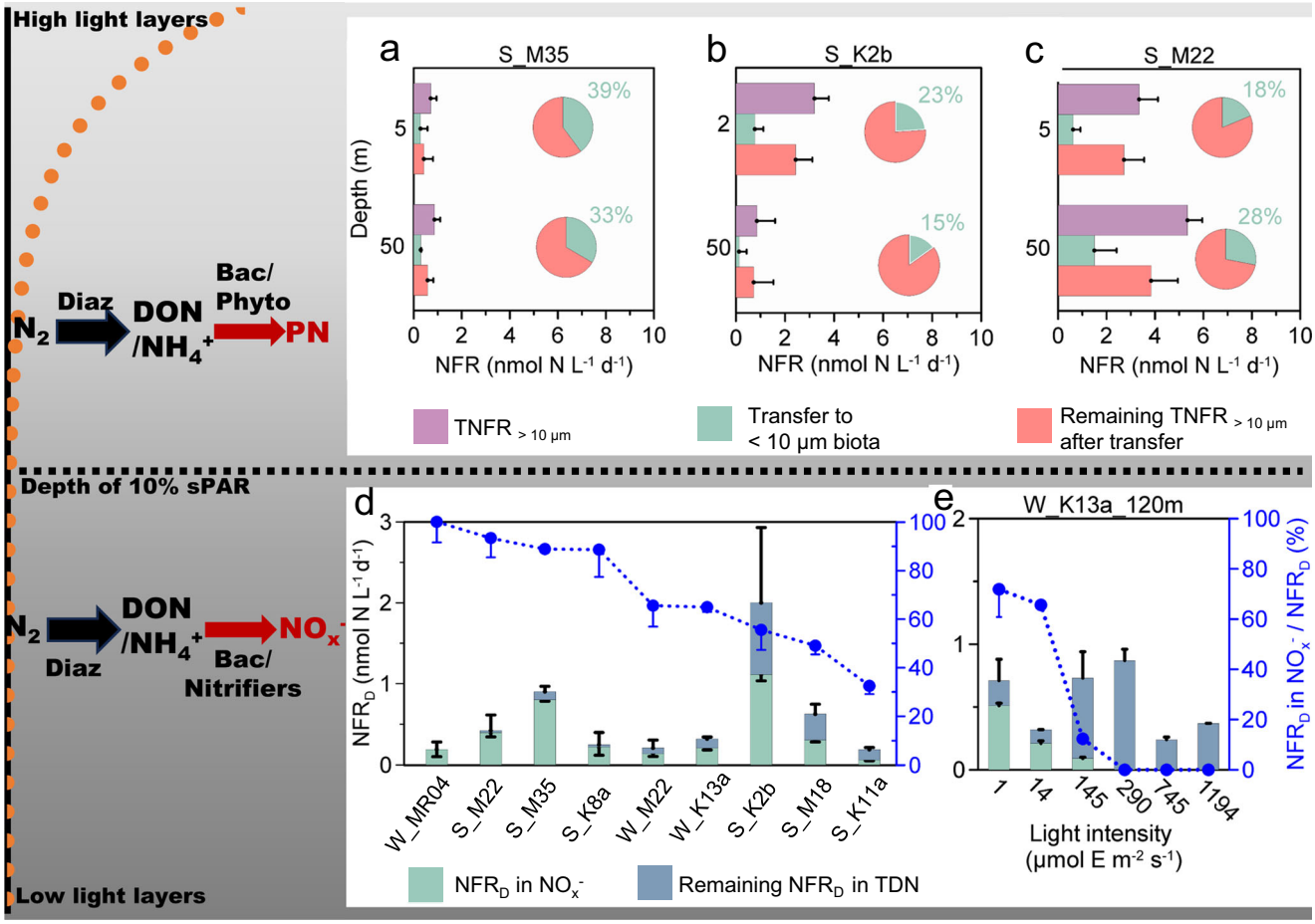

Fig. 3 | The transfer pathways of diazotroph-derived nitrogen (DDN) in the high light layers and low light layers. The upper panel shows the results of size-fractionated experiments in M35 (**a**), K2b (**b**), and M22 (**c**) during the summer cruise. The purple, green, and orange bars represent total nitrogen fixation rates derived from large-sized diazotrophs ($TNFR_{>10\,\mu m}$), released DDN that is partially transferred to small-sized biota (<10 μm), and the remaining DDN derived from large-sized diazotroph after transfer. Data are derived from the subtraction of the data in Supplementary Fig. 11 and presented as mean values + standard deviation. The error bars are propagated standard deviation derived from triplicate rate measurements ($n = 3$ biologically independent samples). The pie charts display the relative distribution of released DDN transferred to small-sized biota and remaining DDN derived from large-sized diazotroph after transfer. The lower panel shows nitrogen fixation rates in dissolved fraction (NFR_D) within NO_x^- fraction and the ratio of NFR_D in NO_x^- fraction to total NFR_D from in situ observations in the low light layers at the nine stations (**d**) and light manipulation experiments at 120 m in K13a during the winter cruise (**e**). The cyan bars are NFR_D in NO_X^- fraction. Data are presented as mean values – standard deviation. The error bars depict one standard deviation from triplicate rate measurements ($n = 3$ biologically independent samples). The blue bars represent the remaining NFR_D in total dissolved nitrogen (TDN). Data are presented as mean values + standard deviation. The error bars are propagated standard deviation derived from triplicate rate measurements ($n = 3$ biologically independent samples). The deep blue dots are the ratio of NFR_D in NO_X^- fraction to the total NFR_D. Data are presented as mean values – standard error of mean. The error bars are standard error of mean, with propagated standard deviation derived from triplicate rate measurements ($n = 3$ biologically independent samples). The stations in chart (**d**) are rearranged according to the ratio. Black arrows show DDN release, and red arrows show DDN transfer. DON, dissolved organic nitrogen; Diaz, diazotrophs; Bac, bacteria; Phyto, phytoplankton; sPAR, surface photosynthetically active radiation; Source data are provided as a Source Data file.

suggesting overestimations in oceanic new production due to nitrification[38,39], particularly in the lower euphotic zone. Moreover, the recycling processes in the lower euphotic zone produce N_2O, offsetting some of the carbon export driven by nitrogen fixation in terms of net greenhouse gas potential[40], which further complicates the role of current findings.

In conclusion, our study underscores the critical role of NFR_D in the marine nitrogen budget through comprehensive observations on diazotrophs and nitrogen fixation rates in the NPSG. NFR_D emerges from the interplay between diazotrophs (as sources/release process) and surrounding organisms (as recipients/transfer process), regulated by their physiological traits and light intensity. The released DDN exhibits high bioavailability and rapid turnover, traversing distinct pathways modulated by light intensity-driven niches. In the high-light layer, released DDN is transferred mainly to phytoplankton, while in the low-light layer, it is utilized by nitrifiers. Our study elucidates the intricate dynamics of nitrogen cycling within the euphotic zone and emphasizes the pivotal role of diazotrophs as keystone species in oligotrophic marine ecosystems.

Methods

Sampling information

Two cruises were conducted onboard R/V Tan Kah Kee from July 2 to August 23, 2020 (KK2003, the summer cruise) and from 23 December 2020 to February 07, 2021 (KK2007, the winter cruise) in the NPSG. Hydrographic data were recorded using SeaBird SBE 911plus CTD system, equipped with temperature, salinity, fluorescence, and photosynthetically active radiation (PAR) sensors. The stations covered a broad range of hydrographic conditions in the NPSG, notably characterized by low surface chlorophyll *a* concentration. Stations were further categorized into the southern, central, and northern NPSG based on both hydrographic and geographic disparities

(Supplementary Fig. 1). The depth of the mixed layer was defined as the depth where a 0.8 °C deviation relative to the surface value we observed[41]. The base of the euphotic zone was defined as the depth with 0.1% surface PAR[42]. Three or four layers were selected in each station within the euphotic zone, determined by the in situ light intensity (Supplementary Fig. 1). Water samples were collected using 12 L Niskin bottles affixed to the CTD rosette.

Pilot tests of method of nitrogen fixation rates incubation

Before commencing the incubation to determine nitrogen fixation rates, we conducted two pre-experiments. First, we assessed the potential contamination of bioavailable non-N_2-^{15}N from commercial $^{15}N_2$ gas. Briefly, triplicate 2 mL of $^{15}N_2$ gas (98.9% atom ^{15}N, chemical purity >99.9%, Cambridge Isotope Laboratories, Inc. Lot. #AR0483820 (gas 1) for the summer cruise and & Lot. #AR0664758 (gas 2) for the winter cruise) were injected into 12 mL tubes (Exetainers, Labco) along with 10 mL of natural particulate-free sea surface water from the NPSG. These tubes were sealed with septum caps and shaken overnight. Subsequently, the $\delta^{15}N$ of total dissolved nitrogen (TDN) in these tubes was measured by the method described below and compared with the natural $\delta^{15}N_{TDN}$ of surface seawater samples (without $^{15}N_2$ gas addition). The $\delta^{15}N_{TDN}$ values for the test seawaters with gas1 and gas2 were 4.8 ± 0.1‰ ($n = 3$ biologically independent samples) and 4.9 ± 0.1‰ ($n = 3$ biologically independent samples), respectively, while the $\delta^{15}N_{TDN}$ values for the natural sample were 4.8‰ ($n = 1$). The result indicated that the two $^{15}N_2$ gases used were free from non-targeted ^{15}N contamination.

Second, we employed a modified bubble release method to add $^{15}N_2$ gas[43]. A pre-experiment was conducted to determine the time required for gas equilibrium and incubation. In brief, at a room temperature of ~25 °C, 4 mL of $^{15}N_2$ gas was injected by syringe through septum caps into thirty-six 4.5 L polycarbonate (PC) bottles filled with sea surface water. These bottles were then subjected to rotation using a self-developed rotating device (~1 rev/s) for durations of 5, 10, 15, and 30 min to facilitate gas equilibration between $^{15}N_2$ and $^{14}N_2$. Afterward, additional sea water was swiftly added into the headspace to halt gas equilibrium. The bottles were then divided into three sets, each with 9 bottles, for incubation periods of 0 h (T0), 24 h (T1), and 48 h (T2), respectively. The $^{15}N_2$ enrichment in the bottles post-incubation was directly measured by membrane inlet mass spectrometry (MIMS). At T0, the $^{15}N_2$-enrichment increased with rotation time, and the percentage of actual $^{15}N_2$ gas dissolution to theoretical dissolution reached 96% after 30 min of rotation (Supplementary Fig. 2a). The $^{15}N_2$-enrichment remained stable between T0 and T1 but decreased at T2 (Supplementary Fig. 2b). Based on these results, we selected a rotation time of 30 min and an incubation time of 24 h for subsequent experiments.

In situ nitrogen fixation rates incubation

The samples collected for in situ nitrogen fixation rates incubation were sub-sampled into four 4.5 L PC bottles that had been pre-rinsed by 1 N HCl. Nitrogen fixation rates were determined using the $^{15}N_2$ labeling method combined with the modified bubble release method[43]. In every layer, 4 mL of $^{15}N_2$ gas was injected into four bottles for incubation via syringe through septum caps, followed by rotation for 30 min (~1 rev/s) in a dark environment. Subsequently, in situ seawater was promptly added into the headspace to cease gas equilibration.

Concurrently, control incubations without $^{15}N_2$ labeling were carried out in each layer. The samples for control incubations were sub-sampled into three 1.25 L PC bottles that had been pre-rinsed with 1 N HCl. The particulate organic nitrogen (PN) and TDN samples in the control group at T0 were treated as natural samples. These control experiments aimed to assess any alterations in $\delta^{15}N_{PN}$ or $\delta^{15}N_{TDN}$ over the incubation periods or potential contamination in subsequent sample-handling processes.

All nitrogen fixation rate incubations (including the control group) in this study were performed using an artificial simulated periodical sunlight system (Hydra® 64HD, Aquallumination) and temperature-controlled incubators. The light intensity and temperature setting closely mimicked in situ conditions (Supplementary Table 1). The incubation duration was 24 h, comprising 12 h of periodical artificial simulated sunlight and 12 h of darkness.

Post-incubation, water from each labeled bottle was subsampled into 12 mL tubes (Exetainers, Labco), fixed with 0.1 mL saturated $HgCl_2$ solution, and to determine the final $^{15}N_2$-enrichment, directly measured by MIMS. The $^{15}N_2$-enrichment ranged from 7.02% to 10.34% (with an average of 9.0 ± 0.6%, $n = 333$ biologically independent samples) in all of our samples. These values surpassed those reported in previous studies, for instance, 2.4 ± 0.2 % ($n = 10$ biologically independent samples) in Bonnet et al.[17] and 1.4 ± 0.1% ($n = 17$ biologically independent samples) in Wen et al.[23]. The elevated $^{15}N_2$-enrichment potentially contributes to higher nitrogen fixation signals, significantly reducing detection limitations.

One sample (T0) and triplicated samples (T1) were collected in the nitrogen fixation rates incubation. Similarly, one sample (T0) and duplicated samples (T1) in the control group incubation were collected. PN samples at T0 and T1 were filtered (<200 mm Hg) using pre-combusted (450 °C, 4 h) 25 mm 0.3 µm glass fiber filters (GF/75; Advantec). TDN samples at T0 and T1 were filtered through a 0.22 µm syringe filter into a 50 mL centrifuge tube (BD Falcon). All filters and dissolved samples were stored at −20°C on board for subsequent analysis.

Light manipulation experiments

Light manipulation incubations were performed at four depths across three stations (M30, M18, and K13a) in the winter cruise. At each depth, alongside the in situ light intensity, four or five gradients of light intensities were established concurrently during the incubation by the artificial simulated periodical sunlight system. All other procedures during the incubation remained the same as those described above. The data of NFR_P in the light manipulation incubations in K13a were described by ref. 44.

Size-fractionated experiments

We conduct size-fractionated incubations at three or four depths across three stations (M35, K2b, and M22) in the summer cruise. The incubations consisted of two parts (Supplementary Fig. 3) as below.

In Part1, as part of the in situ nitrogen fixation rates incubation, subsamples of 2 L water from the 4.5 L bottles after incubation were filtered through 47 mm 10 µm PC filters (Isopore™). Then the filtrate was filtered (under <200 mm Hg pressure) through pre-combusted (450 °C, 4 h) 25 mm 0.3µm GF/75 filters (Advantec). The remaining water (2.5 L) in 4.5 L bottles was directly filtered through 25 mm GF/75 filters and 50 mL water in it was filtered through 0.22 µm syringe filter to determine the in situ bulk nitrogen fixation rates ($TNFR_{bulk}$) as described above.

In the Part2, prior to the incubation, we conducted another parallel incubation. Water samples pre-filtered through 47 mm 10 µm PC filters (Isopore™) were sub-sampled into four 1.25 L PC bottles that had been pre-rinsed by 1 N HCl. The subsequent steps in the incubation process remained consistent with those described above except adding 1 mL of $^{15}N_2$ gas into 1.25 L PC bottles. The particulate and dissolved samples obtained from this incubation were collected for further sample treatment.

PN & TDN concentration and $\delta^{15}N$-PN & $\delta^{15}N$-TDN determination

All filters underwent a freeze-drying process for 48 h before measurement. PN and TDN were oxidized to nitrate using the wet digestion method with slight modifications[45]. Filters and 5 mL Milli-Q (MQ) water or 5 mL TDN samples were placed into 12 mL pre-combusted (450 °C,

4 h) borosilicate glass tubes containing 0.3 mL of purified persulfate oxidizing reagent (POR). The persulfate (ACS-grade, Merck, German) was recrystallized at least three times, then NaOH (ACS-grade, Merck, German) and MQ water were added in a ratio of 6 g persulfate, 6 g NaOH, and 100 mL MQ water. The N in the POR was measured to ensure N concentration was less than 2 μmol N L^{-1} (regent blank). After adding the regent, screw caps were tightly closed, and the tubes were autoclaved at 120 °C for one hour. Nitrate concentration after oxidation (including the particulate sample or TDN, regent blank, and filter blank) was measured using the chemiluminescence method[46]. The blank of filters used during the cruises was less than 6 nmol N. The regent blank and filter blank accounted for <1% and 3% of the total N content in tubes, respectively. Isotopic values (PN, TDN, and NO_x^-) were measured using the denitrifier method coupled with the Gasbench-Isotopic Ratio Mass Spectrometer (IRMS, Thermo Fisher Delta V)[47,48]. The nitrogen isotope data were collected by GC-IRMS software Isodat version 3.0 (Thermo Fisher Scientific). The isotopic values of the regents were also measured. International isotopic standards of NO_3^-, including USGS34, IAEA3, and USGS32, were used to calibrate the δ^{15}N-NO_x^-. The accuracy (standard deviation) was better than ±0.3‰ according to analyses of these standards at a level of 20 nmol N.

Rates calculation

The NFR_P were calculated according to Montoya et al.[49]. The NFR_D was calculated according to Bonnet et al.[16]. The nitrogen fixation rates in the NO_x^- fraction were calculated according to Wan et al.[20].

$$NFR_P = \frac{1}{\triangle T} \times \frac{APN_f - APN_0}{AN_2 - APN_0} \times \frac{PN_f + PN_0}{2} \quad (1)$$

$$NFR_D = \frac{1}{\triangle T} \times \frac{TDN_f \times (ATDN_f - ATDN_0)}{AN_2} \quad (2)$$

$$NFR_{NO_x^-} = \frac{1}{\triangle T} \times \frac{NO_{x\,f}^- \times (ANO_{x\,f}^- - ANO_{x\,0}^-)}{AN_2} \quad (3)$$

NFR_P is the nitrogen fixation rates in the particulate fraction in nmol N L^{-1} d^{-1}; APN_0 and APN_f are the initial and final ratio of ^{15}N% of the PN samples (calculated from the measured isotopic value); PN_0 and PN_f is the initial and final concentration of particulate nitrogen. AN_2 is $^{15}N_2$ enrichment in incubation bottles; ΔT is incubation length (24 h).

NFR_D is the nitrogen fixation rate in the dissolved fraction in nmol N L^{-1} d^{-1}; $ATDN_0$ and $ATDN_f$ are the initial and final ratio of ^{15}N% of the TDN samples (calculated by the measured nitrogen isotopic values); TDN_f is the final concentration of TDN.

NFR_{NOx^-} is the NFR_D in the NO_x^- fraction in nmol N L^{-1} d^{-1}; $ANO_x^-{}_0$ and $ANO_x^-{}_f$ are the initial and final ratio of ^{15}N% of the NO_x^- samples (calculated from the measured isotopic value); $NO_x^-{}_f$ is the final concentration of NO_x^-.

The TNFR was calculated by NFR_P plus NFR_D. The trapezoidal integration method was used to integrate particulate and dissolved nitrogen fixation rates ($INFR_P$ and $INFR_D$) of the water column. The total integrated nitrogen fixation rates were calculated by $INFR_P$ plus $INFR_D$.

Rates detection limitation

The reliable nitrogen fixation rates were determined based on the isotopic change of PN or TDN exceeding the minimum acceptable change. The minimum acceptable change for δ^{15}N-PN or TDN was set to be the average plus three times the standard deviation (SD) of $\delta^{15}N_{PN}$ or $\delta^{15}N_{TDN}$. Since we only collected one PN or TDN sample at T0, the average SD of δ^{15}N-PN or TDN was derived from the three-repeat determination of this single sample at T0, resulting in an SD of 0.3 ‰ for both $\delta^{15}N_{PN}$ and $\delta^{15}N_{TDN}$. The detection limits of NFR_P and NFR_D in each layer were calculated using the data in Supplementary Fig. 12 and were presented in Supplementary Table 1.

In the control experiment, the change in $\delta^{15}N_{PN}$ or $\delta^{15}N_{TDN}$ between T0 and T1 was consistently below 0.9 ‰, suggesting that our subsequent sample treatment processes did not introduce contamination (Supplementary Table 8).

In in situ incubations, all δ^{15}N-PN differences between T0 and T1 at each layer exceeded 0.9‰, indicating that the NFR_P was above detection limitations. However, the NFR_D in S_M35_90m, S_WPS_140m, S_K11a_5m, and W_MR05_5m were below the detection limitations (Supplementary Table 9).

As for NFR_D in NO_x^- fraction in low light layers, the changes of $\delta^{15}NO_x^-$ between T0 and T1 in the control group were always below 0.9 ‰, while $\delta^{15}NO_x^-$ substantially increased in the in situ incubation, indicating that the NFR_D in NO_x^- fraction in the low light layers were detectable at the nine stations (Supplementary Table 4).

Light response curves for total nitrogen fixation

We follow the photosynthetic model proposed by Platt et al. [50]:

$$TNFR = TNFR_{max} \times \left[1 - e^{-\alpha I/TNFR_{max}}\right] \times e^{-\beta I/TNFR_{max}} \quad (4)$$

where $TNFR_{max}$ is the potential maximum rates of TNFR at light-saturating intensity, I is the incubation light intensity and α is the light affinity coefficient for TNFR. β is the parameter that defining the degree of inhibition at high light intensity. The light saturation coefficient I_k was the light intensity where TNFR is maximal.

Transfer efficiency of released fixed nitrogen

In the size-fractionated incubations, the TNFR in Part2 indicated the TNFR derived from small-sized diazotrophs (<10 μm). The difference between $TNFR_{bulk}$ and $TNFR_{<10\,\mu m}$ represented the TNFR derived from large-sized diazotrophs (>10 μm). Additionally, in Part 1, the NFR_{P1} derived from the filtered 10 μm treatment group indicated the nitrogen fixation rates in particulate fraction for small-sized diazotrophs (NFR_{P2}) plus the transfer of released fixed nitrogen from large-sized diazotrophs to the small-sized biota (including diazotrophs and non-diazotrophs). Therefore, the transfer efficiency was calculated as Eq. (5). This method specifically quantifies the transfer efficiency of large-sized diazotrophs (>10 μm) but not that of small-sized diazotrophs.

The transfer efficiency of released fixed nitrogen derived from large-sized diazotroph (>10 μm) into small-sized surrounding biota (<10 μm) was calculated as below:

$$Transferefficiency(\%) = \frac{NFR_{P1} - NFR_{P2}}{TNFR_{Bulk} - TNFR_{<10\mu m}} \times 100\% \quad (5)$$

NFR_{P1} is the nitrogen fixation rates in particulate fraction in incubation of Part 1. NFR_{P2} is the nitrogen fixation rates in particulate fraction in incubation of Part 2. $TNFR_{Bulk}$ is the total nitrogen fixation rates in in situ incubation. $TNFR_{<10\mu m}$ is the total nitrogen fixation rates derived from small-sized diazotrophs in incubation of Part 2 in Supplementary Fig. 3.

The *nifH* gene copies measurements

The samples collected for *nifH* gene copies measurements were from the same cast for rates incubation. In brief, 4 L seawater was filtered through 0.22 μm pore size PC filters (Supor-200, Pall Gelman) for DNA extraction. All filters were promptly flash-frozen in liquid nitrogen and then transferred to −80 °C on board until further analysis. DNA extraction was performed using the phenol-chloroform-isoamyl alcohol method with minor modifications[51]. The concentration and purity of the genomic DNA were detected using a NanoDrop spectrophotometer (Thermo Scientific 2000/2000c). This study targeted

quantification of nine major diazotrophic groups (UCYN-A1, UCYN-A2, UCYN-B, UCYN-C, *Trichodesmium*, Het1, Het2, Het3, γ-24774A11) via TaqMan qPCR assays, employing specific primer and probe sets as per previous studies (Supplementary Table 10). Each 20 μL reaction mixture contained 10 μL of Premix Ex Taq (probe qPCR; Takara Bio Inc.), 400 nmol L^{-1} of fluorogenic probe, 400 nmol L^{-1} each of the forward and reverse primers, and 1 μL of environmental DNA. The thermocycling conditions were 50 °C for 2 min, 95 °C for 2 min, and 45 cycles of 95 °C for 15 s, followed by 60 °C for 1 min. Triplicate qPCRs were run for each environmental DNA sample and for each standard on a CFX96 Real-Time System (Bio-Rad Laboratories). Negative controls without templates were also included to test for contamination. Linearized plasmid standards were generated by stepwise dilutions for each qPCR run and were used to calculate copies for each sample. The amplification efficiencies of PCR consistently ranged between 95% and 100%, with R^2 values of standard curves >0.99. The quantification limit of the qPCR reactions was set at one *nifH* gene copy per reaction.

Primary production rate measurements

During the summer cruise, at each station and depth, in situ primary production incubations were conducted simultaneously with in situ nitrogen fixation rate incubations. The $NaH^{13}CO_3$ (99 atom% ^{13}C, Cambridge Isotope Laboratories) solution was injected into each triplicate 4.5 L bottle (final concentration of 100 μmol C L^{-1}). After 24 h of incubation, triplicate water samples were gently filtered (<200 mm Hg) onto precombusted (450 °C, 4 h) 25 mm 0.3μm GF/75 filters (Advantec). The particulate organic carbon (POC) concentrations and isotopic values were analyzed on an EA (Elementar vario PYRO cube) coupled with an IRMS (Isoprime Ltd). International references (USGS40 and USGS41) were inserted every ten samples to check for drift and ensure the accuracy of the measurements. The reproducibility of $\delta^{13}C$ measurements was better than 0.3‰. The primary production rates were calculated using an equation proposed by Hama et al. [52].

$$PP = \frac{1}{\triangle T} \times \frac{APOC_f - APOC_0}{ADIC - APOC_0} \times \frac{POC_f + POC_0}{2} \quad (6)$$

PP is the primary production rate in μmol C L^{-1} d^{-1}; $APOC_0$ and $APOC_f$ are the initial and final ratio of ^{13}C% of the POC samples (calculated from the measured isotopic value); POC_0 and POC_f is the initial and final concentration of POC. ADIC is ^{13}C enrichment in incubation bottles; ΔT is incubation length (24 h).

In situ NO_3^- + NO_2^- (NO_X^-) concentration

The samples collected for determining the in situ nitrate concentration were from the different cast from that for rates incubation. Standard colorimetric techniques were used for the determination of NO_3^- + NO_2^- (NO_x^-) concentrations on board with the same detection limits of 0.03 μmol N L^{-1} [53]. For NO_x^- concentrations falling below the detection limit of the standard colorimetric method, measurements were conducted using a liquid waveguide capillary flow cell with a detection limit of 2.4 nmol N L^{-1} [54]. The nitracline was determined as the midpoint (average) of the steepest nitrate concentration gradient with depths[55].

Statistical analysis

The significance of differences among NFR and environmental parameters in different stations was tested by *t* test and analysis of variance followed by the Tukey test. A significance level of $p < 0.05$ was applied. The analyses were performed using SPSS Statistics 26.

Reporting summary

Further information on research design is available in the Nature Portfolio Reporting Summary linked to this article.

Data availability

Source data are provided in this paper. The data used in this study are available in the Figshare database that can be accessed through https://doi.org/10.6084/m9.figshare.26384017.

References

1. Zehr, J. P. & Capone, D. G. Changing perspectives in marine nitrogen fixation. *Science* **368**, eaay9514 (2020).
2. Böttjer, D. et al. Temporal variability of nitrogen fixation and particulate nitrogen export at station ALOHA. *Limnol. Oceanogr.* **62**, 200–216 (2017).
3. Mills, M. M. & Arrigo, K. R. The magnitude of oceanic nitrogen fixation influenced by the nutrient uptake ratio of phytoplankton. *Nat. Geosci.* **3**, 412–416 (2010).
4. Mulholland, M. R. The fate of nitrogen fixed by diazotrophs in the ocean. *Biogeosciences* **4**, 37–51 (2007).
5. Glibert, P. M. & Bronk, D. A. Release of dissolved organic nitrogen by marine diazotrophic cyanobacteria, *Trichodesmium* spp. *Appl. Environ. Microbiol.* **60**, 3996–4000 (1994).
6. Carpenter, E. J., & Capone, D. G. (Eds.). Marine pelagic cyanobacteria: *trichodesmium* and other diazotrophs 362, *Springer Science & Business Media* (1992).
7. Glibert, P. M., & O'neil, J. M. Dissolved organic nitrogen release and amino acid oxidase activity by *Trichodesmium* spp. *Bull. Inst. océanogr.* 265–272 (1999).
8. Berman-Frank, I., Bidle, K. D., Haramaty, L. & Falkowski, P. G. The demise of the marine cyanobacterium, *Trichodesmium* spp., via an autocatalyzed cell death pathway. *Limnol. Oceanogr.* **49**, 997–1005 (2004).
9. Lu, Y. et al. Effect of light on N_2 fixation and net nitrogen release of *Trichodesmium* in a field study. *Biogeosciences* **15**, 1–12 (2018).
10. Hewson, I., Govil, S. R., Capone, D. G., Carpenter, E. J. & Fuhrman, J. A. Evidence of *Trichodesmium* viral lysis and potential significance for biogeochemical cycling in the oligotrophic ocean. *Aquat. Microb. Ecol.* **36**, 1–8 (2004).
11. O'Neil, J. M. Grazer interactions with nitrogen-fixing marine Cyanobacteria: adaptation for N-acquisition? *Bull. Inst. océanogr.* 293–318 (1999).
12. Fawcett, S. E., Lomas, M. W., Casey, J. R., Ward, B. B. & Sigman, D. M. Assimilation of upwelled nitrate by small eukaryotes in the Sargasso Sea. *Nat. Geosci.* **4**, 717–722 (2011).
13. Hunt, B. P. et al. Contribution and pathways of diazotroph-derived nitrogen to zooplankton during the VAHINE mesocosm experiment in the oligotrophic New Caledonia lagoon. *Biogeosciences* **13**, 3131–3145 (2016).
14. Caffin, M., Berthelot, H., Cornet-Barthaux, V., Barani, A. & Bonnet, S. Transfer of diazotroph-derived nitrogen to the planktonic food web across gradients of N_2 fixation activity and diversity in the western tropical South Pacific Ocean. *Biogeosciences* **15**, 3795–3810 (2018).
15. Mulholland, M. R., Heil, C. A., Bronk, D. A., O'Neil, J. M. & Bernhardt, P. Does nitrogen regeneration from the N_2 fixing cyanobacteria *Trichodesmium* spp. fuel Karenia brevis blooms in the Gulf of Mexico. *Harmful Algae* **47-49**, 2002 (2001).
16. Bonnet, S. et al. Diazotroph derived nitrogen supports diatom growth in the South West Pacific: a quantitative study using nanoSIMS. *Limnol. Oceanogr.* **61**, 1549–1562 (2016).
17. Bonnet, S. et al. Dynamics of N_2 fixation and fate of diazotroph-derived nitrogen in a low-nutrient, low-chlorophyll ecosystem: results from the VAHINE mesocosm experiment (New Caledonia). *Biogeosciences* **13**, 2653–2673 (2016).
18. Shao, Z. et al. Global oceanic diazotroph database version 2 and elevated estimate of global N_2 fixation. *Earth Syst. Sci. Data*, **15**, 3673–3709 (2023).
19. Berthelot, H., Benavides, M., Moisander, P. H., Grosso, O. & Bonnet, S. High-nitrogen fixation rates in the particulate and dissolved pools

in the Western Tropical Pacific (Solomon and Bismarck Seas). *Geophys. Res. Lett.* **44**, 8414–8423 (2017).
20. Wan, X. S. et al. Ambient nitrate switches the ammonium consumption pathway in the euphotic ocean. *Nat. Commun.* **9**, 915 (2018).
21. Lu, Y. et al. Biogeography of N_2 fixation influenced by the western boundary current intrusion in the South China Sea. *J. Geophys. Res. Oceans* **124**, 6983–6996 (2019).
22. Shiozaki, T. et al. Basin scale variability of active diazotrophs and nitrogen fixation in the North Pacific, from the tropics to the subarctic Bering Sea. *Glob. Biogeochem. Cycles* **31**, 996–1009 (2017).
23. Wen, Z. et al. Nutrient regulation of biological nitrogen fixation across the tropical western North Pacific. *Sci. Adv.* **8**, eabl7564 (2022).
24. Gradoville, M. R. et al. Light and depth dependency of nitrogen fixation by the non-photosynthetic, symbiotic cyanobacterium UCYN-A. *Environ. Microbiol.* **23**, 4518–4531 (2021).
25. Garcia, N. S., Fu, F.-X. & Hutchins, D. A. Colimitation of the unicellular photosynthetic diazotroph Crocosphaera watsonii by phosphorus, light, and carbon dioxide. *Limnol. Oceanogr.* **58**, 1501–1512 (2013).
26. Lomas, M. W., Rumbley, C. J. & Glibert, P. M. Ammonium release by nitrogen sufficient diatoms in response to rapid increases in irradiance. *J. Plankton Res.* **22**, 2351–2366 (2000).
27. Hansell, D. A., & Carlson, C. A. (Eds.). Biogeochemistry of marine dissolved organic matter. (*Academic Press*, 2014).
28. Yu-Fang, T., Fei-Jen, L., Chiang, K. P., Kao, S. J. & Shiah, F. K. Potential impacts of N_2-fixing *Trichodesmium* on heterotrophic bacterioplankton turnover rates and organic carbon transfer efficiency in the subtropical oligotrophic ocean system. *TAO: Terr. Atmos. Ocean. Sci.* **16**, 361 (2005).
29. Xu, M. N. et al. Coupled effect of substrate and light on assimilation and oxidation of regenerated nitrogen in the euphotic ocean. *Limnol. Oceanogr.* **64**, 1270–1283 (2019).
30. Deng, L., Cheung, S., Xu, Z., Liu, K. & Liu, H. Microzooplankton grazing exerts a strong top-down control on unicellular cyanobacterial diazotrophs. *J. Geophys. Res. Biogeosci.* **128**, e2023JG007824 (2023).
31. Fuhrman, J. Close coupling between release and uptake of dissolved free amino acids in seawater studied by an isotope dilution approach. *Mar. Ecol. Prog. Ser.* **37**, 45–52 (1987).
32. Adam, B. et al. N_2-fixation, ammonium release and N-transfer to the microbial and classical food web within a plankton community. *ISME J.* **10**, 450–459 (2016).
33. Bronk, D. A., Glibert, P. M., Malone, T. C., Banahan, S. & Sahlsten, E. Inorganic and organic nitrogen cycling in Chesapeake Bay: autotrophic versus heterotrophic processes and relationships to carbon flux. *Aquat. Microb. Ecol.* **15**, 177–189 (1998).
34. Moore, C. M. et al. Processes and patterns of oceanic nutrient limitation. *Nat. Geosci.* **6**, 701–710 (2013).
35. Galloway, J. N. et al. Nitrogen cycles: past, present, and future. *Biogeochemistry* **70**, 153–226 (2004).
36. Codispoti, L. A. et al. The oceanic fixed nitrogen and nitrous oxide budgets: moving targets as we enter the anthropocene? *Sci. Mar.* **65**, 85–105 (2001).
37. Gruber, N. The dynamics of the marine nitrogen cycle and its influence on atmospheric CO_2 variations. *In*: The ocean carbon cycle and climate (pp. 97–148). Springer Netherlands (2004).
38. Yool, A., Martin, A. P., Fernández, C. & Clark, D. R. The significance of nitrification for oceanic new production. *Nature* **447**, 999–1002 (2007).
39. Liu, L. et al. Reduced nitrite accumulation at the primary nitrite maximum in the cyclonic eddies in the western North Pacific subtropical gyre. *Sci. Adv.* **9**, eade2078 (2023).
40. Wan, X. S. et al. Epipelagic nitrous oxide production offsets carbon sequestration by the biological pump. *Nat. Geosci.* **16**, 29–36 (2023).
41. Kara, A. B., Rochford, P. A. & Hurlburt, H. E. An optimal definition for ocean mixed layer depth. *J. Geophys. Res. Oceans* **105**, 16803–16821 (2000).
42. Siegel, D. A., Michaels, A. F., Sorensen, J. C., O'Brien, M. C. & Hammer, M. A. Seasonal variability of light availability and utilization in the Sargasso Sea. *J. Geophys. Res. Oceans* **100**, 8695–8713 (1995).
43. White, A. E. et al. A critical review of the $^{15}N_2$ tracer method to measure diazotrophic production in pelagic ecosystems. *Limnol. Oceanogr. Methods* **18**, 129–147 (2020).
44. Shen, H., et al. Physical optima for nitrogen fixation in cyclonic eddies in the Subtropical Northwestern Pacific. *Prog. Oceanogr.* **226**, 103298 (2024).
45. Knapp, A. N., Sigman, D. M., & Lipschultz, F. N isotopic composition of dissolved organic nitrogen and nitrate at the Bermuda Atlantic time-series Study site. *Glob. Biogeochem. Cycles* **19** (2005).
46. Braman, R. S. & Hendrix, S. A. Nanogram nitrite and nitrate determination in environmental and biological materials by vanadium (III) reduction with chemiluminescence detection. *Anal. Chem.* **61**, 2715–2718 (1989).
47. Casciotti, K. L., Sigman, D. M., Hastings, M. G., Böhlke, J. K. & Hilkert, A. Measurement of the oxygen isotopic composition of nitrate in seawater and freshwater using the denitrifier method. *Anal. Chem.* **74**, 4905–4912 (2002).
48. Sigman, D. M. et al. A bacterial method for the nitrogen isotopic analysis of nitrate in seawater and freshwater. *Anal. Chem.* **73**, 4145–4153 (2001).
49. Montoya, J. P., Voss, M., Kahler, P. & Capone, D. G. A simple, high-precision, high-sensitivity tracer assay for N_2 fixation. *Appl. Environ. Microbiol.* **62**, 986–993 (1996).
50. Platt, T. G. C. L., Gallegos, C. L., & Harrison, W. G. Photoinhibition of photosynthesis in natural assemblages of marine phytoplankton. *J. Mar. Res.* **38** (1980).
51. Chen, M. et al. Biogeographic drivers of diazotrophs in the western Pacific Ocean. *Limnol. Oceanogr.* **64**, 1403–1421 (2019).
52. Hama, T. et al. Measurement of photosynthetic production of a marine phytoplankton population using a stable ^{13}C isotope. *Mar. Biol.* **73**, 31–36 (1983).
53. Han, A. et al. Nutrient dynamics and biological consumption in a large continental shelf system under the influence of both a river plume and coastal upwelling. *Limnol. Oceanogr.* **57**, 486–502 (2012).
54. Du, C. et al. Impact of the Kuroshio intrusion on the nutrient inventory in the upper northern South China Sea: insights from an isopycnal mixing model. *Biogeosciences* **10**, 6419–6432 (2013).
55. Du, C., Liu, Z., Kao, S. J. & Dai, M. Diapycnal fluxes of nutrients in an oligotrophic oceanic regime: the South China Sea. *Geophys. Res. Lett.* **44**, 11–510 (2017).

Acknowledgements

We acknowledge the captain and crew of the R/V *Tan Kah Kee* for their help during the cruises. We thank C. Du for determining nitrate concentrations. We also thank M. Chen and Y. Zhang in assistance of determining *nifH* genes abundance. We acknowledge the NASA Ocean Biology Distributed Active Archive Center for the sea surface chlorophyll-a data. This work was supported by the National Natural Science Foundation of China (grant 92058204 to S.K., grant 42106048 to M.N.X., grant 92258302, and 41721005 to S.K.). X.S.W. acknowledges funding from the Simons Foundation through award No. 675459 (B.B. Ward, PI). S.K. was supported by the Innovational Fund for Scientific and Technological Personnel of Hainan Province, KJRC2023B04.

Author contributions

H.S., X.S.W., and S.K. conceived the idea and designed the experiments. H.S., X.S.W., and W.Z. performed the experiments during the cruises. H.S. processed the samples in the shore lab and obtained data. H.S., X.S.W., M.N.X., and S.K. analyzed the data. H.S. drafted the manuscript and figures with contributions from X.S.W., M.D., M.N.X., and S.K.

Competing interests

The authors declare no competing interests.

Additional information

Supplementary information The online version contains supplementary material available at https://doi.org/10.1038/s41467-024-53067-x.

Correspondence and requests for materials should be addressed to Min N. Xu or Shuh-Ji Kao.

Peer review information *Nature Communications* thanks Ruifeng Zhang and the other, anonymous, reviewers for their contribution to the peer review of this work. A peer review file is available.

Reprints and permissions information is available at http://www.nature.com/reprints

Publisher's note Springer Nature remains neutral with regard to jurisdictional claims in published maps and institutional affiliations.

Open Access This article is licensed under a Creative Commons Attribution-NonCommercial-NoDerivatives 4.0 International License, which permits any non-commercial use, sharing, distribution and reproduction in any medium or format, as long as you give appropriate credit to the original author(s) and the source, provide a link to the Creative Commons licence, and indicate if you modified the licensed material. You do not have permission under this licence to share adapted material derived from this article or parts of it. The images or other third party material in this article are included in the article's Creative Commons licence, unless indicated otherwise in a credit line to the material. If material is not included in the article's Creative Commons licence and your intended use is not permitted by statutory regulation or exceeds the permitted use, you will need to obtain permission directly from the copyright holder. To view a copy of this licence, visit http://creativecommons.org/licenses/by-nc-nd/4.0/.

© The Author(s) 2024